Planetary Atmospheres Minor Species Sensor (PAMSS)

Doug Maukonen, Chris J. Fredricksen, Andrei V. Muraviev, Ammar Alhasan, Seth Calhoun, Guy Zummo, Robert E. Peale, Joshua E. Colwell

University of Central Florida, Orlando FL 32816

ABSTRACT

The Planetary Atmospheres Minor Species Sensor (PAMSS) is an ultra-trace gas sensor. This paper reports its transition from a Technical Readiness Level of 4 (TRL4) to TRL 5 and an established path forward to TRL6. This report describes tests of PAMSS in chambers that simulate a balloon flight to 30 km. Lessons learned inform a number of improvements, which are being implemented for a balloon flight planned for June 2014.

Keywords: Gas sensor, balloon flight

1. INTRODUCTION

Chemical analysis of Earth's atmosphere addresses many important problems. These include ozone and threats to its concentration, air pollution, acid rain, excited metastable species, air glow, climate change, and the climatic impact of trace gases. On other planets, remote and local atmospheric probes have investigated whether life has existed (Mars), runaway greenhouse effects (Venus), exotic atmospheres (Titan), and the structure of deep opaque atmospheres (e.g. Jupiter). A problem is that most atmospheric probes are unable to locally quantify concentrations of trace vapors or gases, which nevertheless may be important to atmospheric chemistry or to questions such as life. It has not been possible to quantify local concentrations when spectroscopic signatures are very weak. Limb sounding and satellite remote sensing integrate over very long path lengths, through a range of altitudes, and over broad areas, so that the obtained data represent a spatial average of concentrations and conditions.

The opportunity described here is infrared intracavity laser absorption spectroscopy. Our system based on this principle and using an infrared quantum cascade laser (QCL) is designated the "Planetary Atmosphere Minor Species Sensor", or PAMSS. PAMSS is a compact system that samples locally while achieving effective optical path lengths of hundreds of kilometers for detection of ultra-trace species at parts per trillion levels. PAMSS may be tailored for sensing any molecule that has an infrared absorption band, namely any molecule except for homopolar diatomic molecules such as H_2, N_2, and O_2. The details concerning the construction and principles of PAMSS, together with first sensitivity results, are reported in Ref. [1].

2. RESULTS OF FLIGHT SIMULATION TEST

On 10 DEC 2013, PAMSS was tested inside the environmental chamber at Near Space Corporation (NSC) in Tillamook OR. This section describes the system that was prepared and results of that test. Fig. 1 presents a photograph of the assembled PAMSS system on 7 DEC 2013 in the lab at UCF, before the trip to Oregon. The system at this point is at TRL4. PAMSS was subsequently partially disassembled for packing into two standard rolling carry-on suitcases. The chassis was about ¾ inch too long to fit comfortably in the suitcase, so that the end members had to be removed. Test electronics and back-up parts were packed into a third suitcase and a laptop was carried separately. This method of

travel proved safe for the system, and caused only a little inconvenience at the security check point. We did not attempt to transport batteries or chemicals.

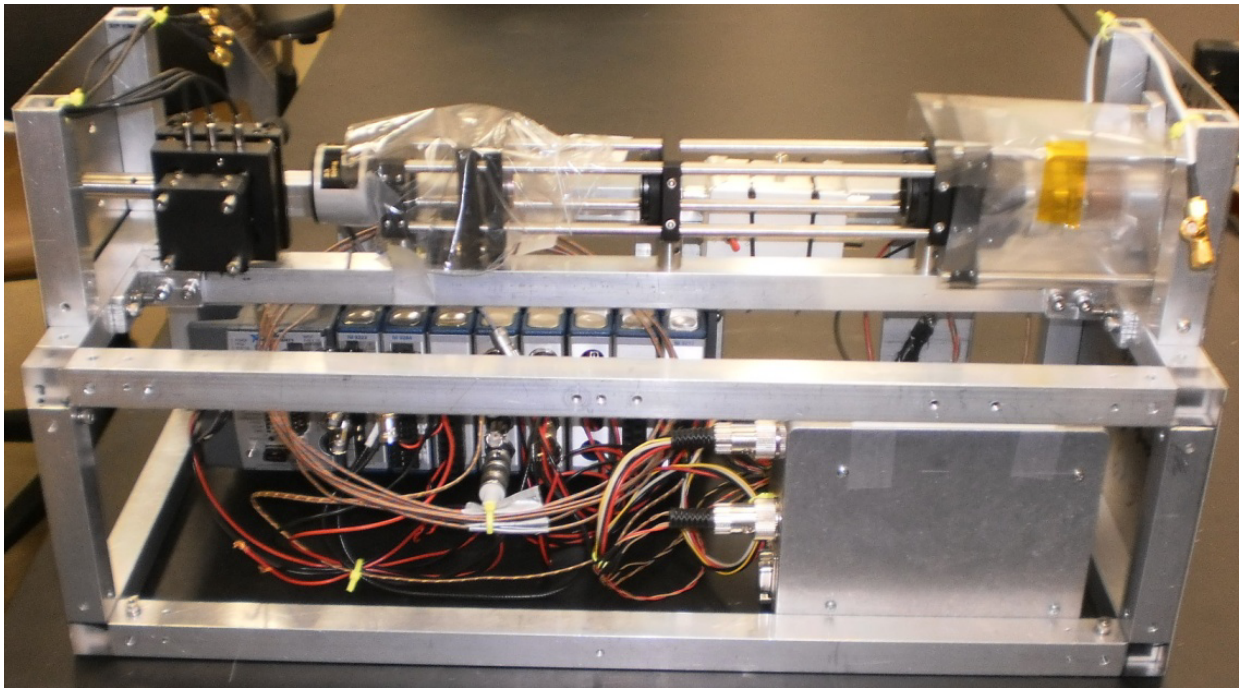

Figure 1: Photographs of completed PAMSS system in UCF lab before the test.

Weigh-in was performed at NSC on 9 DEC 2013 after reassembly. The weight of the complete system minus batteries and some cables was 7.95 kg. When batteries are added, the projected weight will be just under 10 kg, which is within specifications. NSC reports that their balloon as somewhat more capacity than 10 kg.

Fig. 2 presents a photograph of PAMSS loaded into the environmental test chamber at NSC. This consisted of a rectangular metal box with a heavy transparent plexiglass door on hinges and sealed via an o-ring. The chamber is pumped down slowly via a small rotary pump, and an electronic readout gives the pressure in mbar. The experiment rests on a thick metal baseplate, to the underside of which copper cooling coils are attached. Liquid nitrogen is passed through these coils, and a solenoid valve automatically regulates the flow via an on-off controller. The experiment is surrounded by a rectangular sheet-copper shroud, which is attached to the base-plate and is cooled by conduction. The experiment sits on Styrofoam blocks to avoid directly cooling the chassis, so that the experiment is cooled radiatively and by conduction via the rarified atmosphere. The front of the copper enclosure remained open to 300 K radiation from the plexiglass. Electrical connections are made via a DB-25 vacuum feedthrough connection welded into a circular flange mounted on top of the chamber. Additionally, there was a single BNC connection feedthrough. NSC provided several thermocouples for monitoring the temperature at various locations, and we had several of our own integrated into PAMSS.

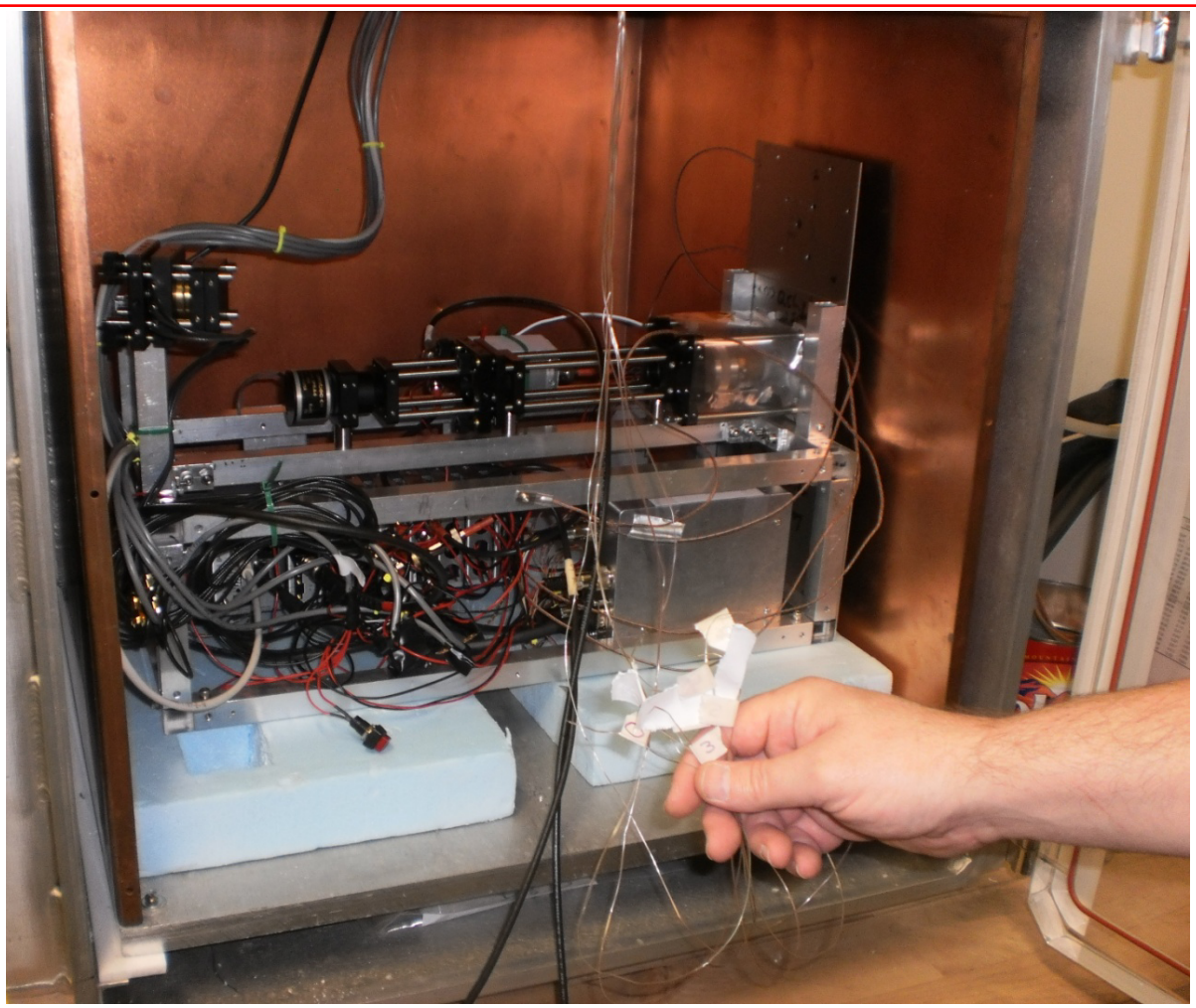

Figure 2. PAMSS loaded into NRC test chamber.

Fig. 3 presents plots of chamber pressure and some of the critical temperatures recorded by hand from the read-outs during the experiment. Data were also logged electronically, but these show nothing different. Letters above the inverted triangles signify events during the experiment, as follows.

At event “a”, the 12 V laser PS and 9 V TEC PS were unplugged. This was done because the hot side of the TEC had reached a dangerously high temperature (near 100 C), and because the laser had reached 26 C and was no longer emitting. By 30 min into the experiment the pressure had dropped to the equivalent of 100000 ft altitude (13 mbar), but the ambient temperature was still 13 C. After event “a”, the hot and cold sides of the TEC approached equilibrium, and the laser reached a maximum temperature of 48 C, before both sides cooled back to 28 C, where it was again safe to operate the TEC.

At event “b”, we restarted the TEC and laser excitation. The laser temperature dropped to 16 C within 7 minutes before starting to heat up again. The laser emission was restored, but there was some instability, i.e. the laser sometimes missed a shot. This was identified as due to noise coming from the pulse width modulation in the TEC controller, as discussed below.

The laser continued to heat up. At event “c”, we again unplugged the laser and TEC to avoid overheating.

When the laser temperature had returned to 28.4 C, we again restarted the laser and TEC by plugging in their power supplies at event "d". Laser emission was again observed. The TEC-controller-caused noise reappeared, with the same emission pulse instability observed.

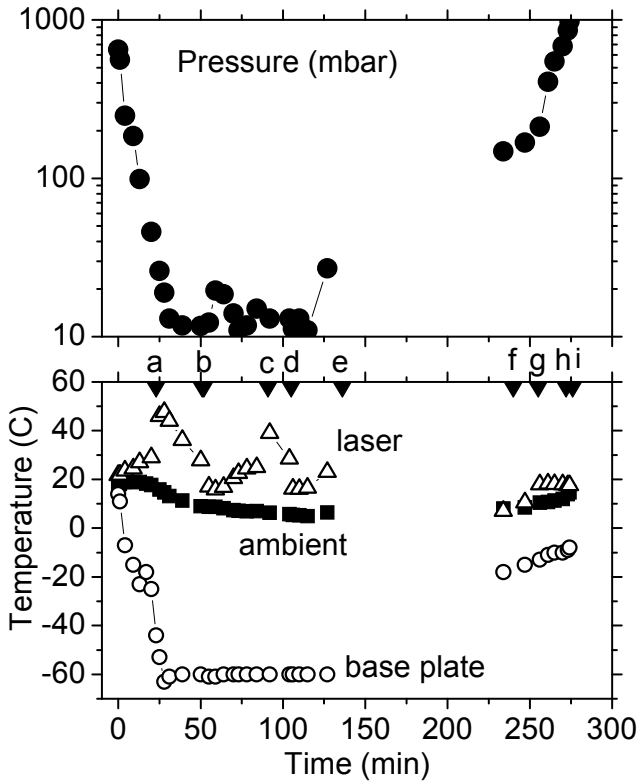

Figure 3. Chamber pressure (top) and some key temperatures (bottom) as a function of time. Letters and solid triangle symbols signify particular events described in the text.

At event "e", the laser and TEC power supplies were again unplugged to avoid overheating. We turned off the LN_2 supply and the vacuum pump, but we left the system under vacuum. We broke for lunch.

When we returned from lunch, the laser temperature had reached 7 C, and the pressure had risen to 100 mbar, but the ambient temperature was still only 8 C due to the large thermal capacitance of the cold base plate. At event "f" the laser and TEC power supplies were plugged in again. The laser current was increased in steps from 0.3 to 0.9 amps at 10 Hz rep rate with 8 ms pulse duration, where strong laser emission was observed. Then, the rep rate was increased to 25 Hz to help warm the laser back to ambient temperature. However, the electrical power dissipated by the laser heats it only very slowly. The main cause of overheating is evidently inefficient dissipation of heat from the hot side of the TEC, causing the TEC to have to work harder to maintain the set point temperature difference. The TEC heats itself, and later experiments determined the specific brand of TEC we were using was very inefficient. The slope of the temperature vs. time curve can be used to determine the thermal capacitance of the cold plate. At event "g", we started leaking in air, while continuing to operate the laser, which held a stable temperature of about 18 C.

At event "h", the chamber was opened. The metal chassis felt cold and slightly damp. Readjusting the alignment increased the laser intensity by tenfold, and the laser emission was stable. We ended the experiment at event "i" and started packing.

One of the concerns that we had was that temperature cycling might cause damage to the anti-reflection coating on the front facet of the laser. A corner of the coating had already peeled up when the laser was delivered new. Just before the chamber test, we noticed some new damage. The end facet was imaged again after the experiment, but no difference was observed, as shown in Fig. 7.

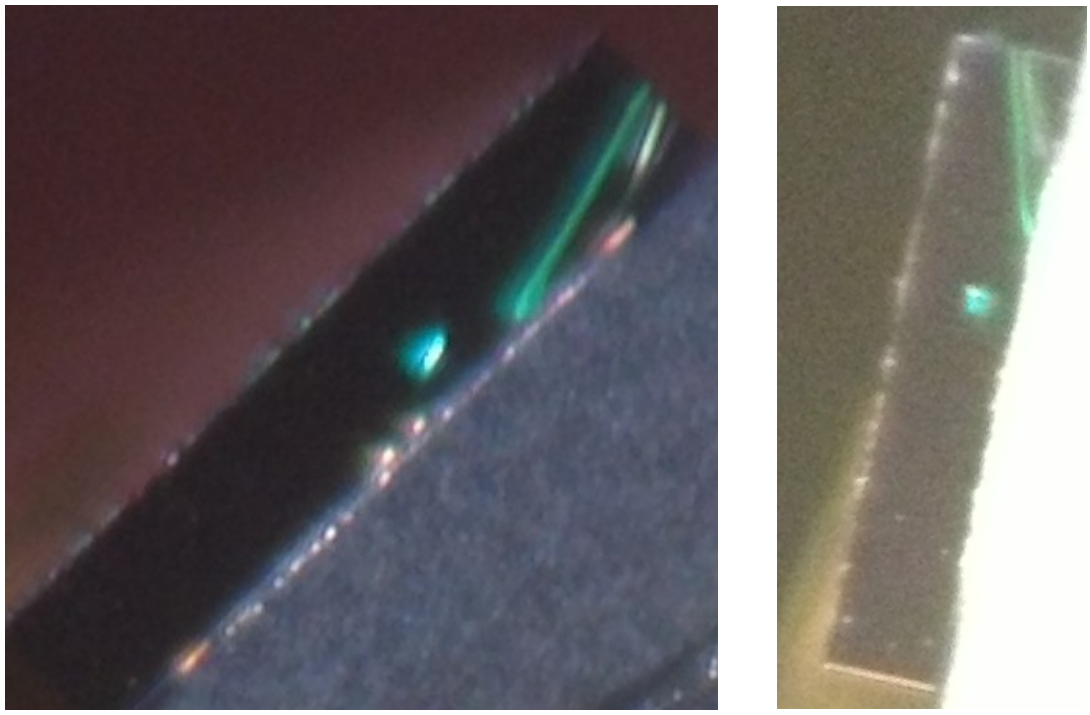

Figure 4. Microphotographs of QCL end facet (left) before test, and (right) after test. The bright line in the upper corner is AR coating damage as delivered. The bright spot in the middle of the facet is coating damage that appeared just before the chamber test. There appears to be no increase in the damage caused by the test.

3. LESSONS LEARNED AND PROPOSED IMPROVEMENTS

Fixing the laser mount rigidly to the system chassis makes some sense for thermal management, but loss in the alignment degrees of freedom proved to be a problem. This is because the QCL as delivered by the vendor is not soldered squarely in its mount. To compensate for this misalignment, a piece of copper tape was used as a shim under edge of the laser mount. However, this crude solution did not achieve the most optimum alignment.

We have implemented a custom mount for the QCL that allows angle adjustment, following the design of standard commercially available mirror mounts. Fig. 5 (left) presents a photograph. Three micrometer screws attached the aluminum plate push against spring tension on the black anodized aluminum plate, which is attached to the system frame. Fig. 5 right shows the mount for the laser. Two copper blocks are connected via a new and more efficient thermo-electric cooler element (Thorlabs). Thermisters are epoxied to these blocks. The laser's mount is attached to the right block. The left block, which is the hot side, is attached to a black anodized radiator. The radiator is attached to threaded holes in the adjustable mount (Fig. 5, left) via two machine screws.

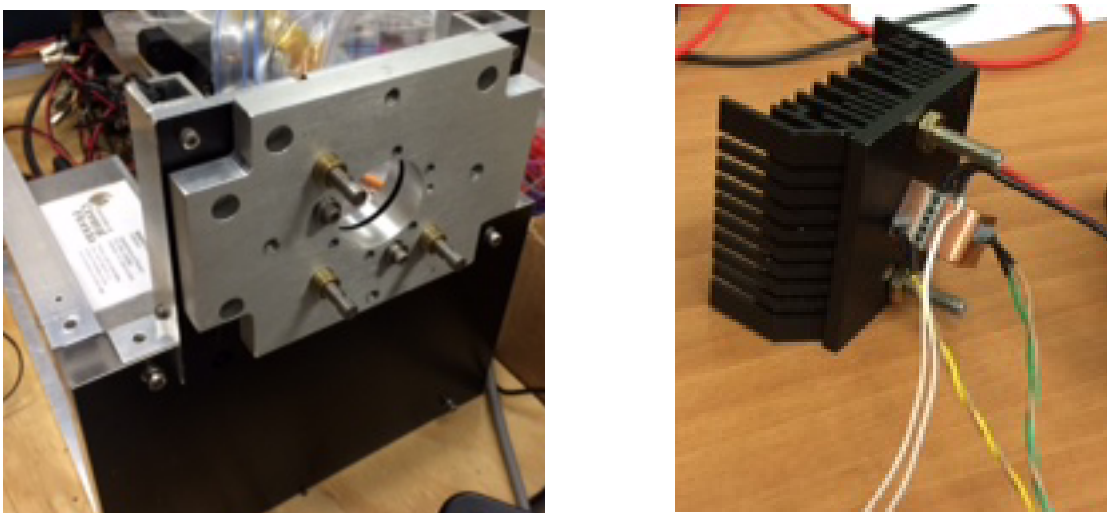

Fig. 5 Photographs of (left) adjustable laser mount and (right) thermal management system for the QCL.

The radiation plate used in our test proved inadequate to the heat load. We found that the TEC element we were using was most of the problem, as it was very inefficient and overheated by itself. Replacing the TEC with one from Thorlabs optimized to cool lasers seems to have solved the problem.

The ambient temperature in the chamber was strongly influenced by the amount of heat generated by our instrument and the inefficiency of cooling. Thermal deformation of the optical cage rail system is one of the main concerns, but this part of PAMSS never made it to -60 C, only to 4 C. Thus, the test was inconclusive regarding thermal expansion issues.

We started operating the laser driver with a 9 V power supply. The QCL driver would not go above 5.6 V, even with a dummy load. Though the driver chip is specified to run at 9 V, we were not able to reach the laser operating current. Changing the laser power supply to a 12 V unit solved this problem. This indicates that we must have 12 V available in our battery system to operate the laser, while the TEC and everything else operate fine with 9 V.

We noticed 1 V AC between different grounds from different parts of the chassis. Connecting the grounds of our two 9V supplies reduced the AC signal to 300 mV. A single system power supply with single ground is needed.

Each time the TEC was restarted (events b, d, and f) after the hot and cold sides of the TEC had returned to ~28 C, strong digital noise of 1 kHz repetition rate was observed on the applied laser voltage. The TEC operates at 1 kHz, and while the system is still cool, it controls the temperature by means of pulse width modulation. We noticed that the noise disappeared as soon as the laser reached 20 C, when the TEC controller started applying continuous power. If this is due to grounding problems, it is an additional suggestion that we need to run off a single power supply (instead of the three we were using, one 12 V for the laser, one 9 V for the TEC, and on 9 V for everything else.)

Fig. 3 shows that the ambient temperature in the NSC environmental chamber never fell below 8 C. This is due to poor thermal flow through the thin Cu shroud and leaving one face of the shroud wide open to 300 K radiation from the Plexiglas door. After our return from NSC, we immediately began preparing our own environmental test chamber. Fig. 6 presents a photograph of our chamber. It consists of a former thermal evaporation system with a large steel bell jar 0.5 m diameter and 0.8 m height. PAMSS is mounted vertically inside the bell jar. Our roughing pump has much higher pumping rate than the one used at NSC, allowing us to rapidly reach 13 mbar or even lower. Cooling is provided by a copper shroud with cooling over its entire surface via liquid nitrogren (LN_2) coils. Feed-throughs with thin-wall stainless tube standoff-shrouds were fabricated and attached to the evaporator base plate to allow introduction of LN_2 without freezing the rubber o-ring seal. Additional feed-through was made available for electrical connections.

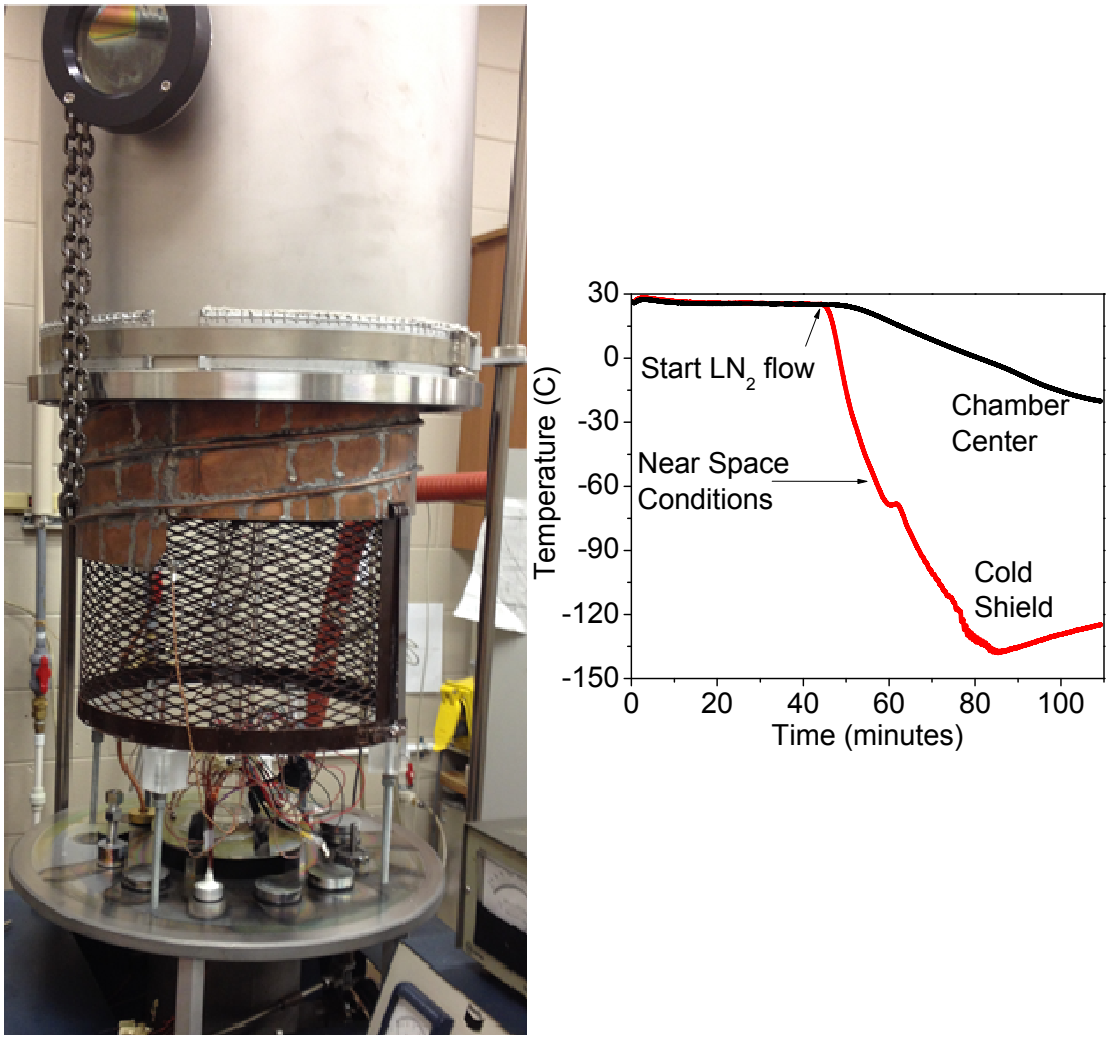

Figure 6. UCF environmental test chamber. (right) Temperatures measured in the UCF space-simulating environmental chamber. The pressure was < 1 Torr.

Fig. 6 (right) presents first cooling data for the Cu shroud and for a point at the center of the chamber. The cold shield was connected to the fully opened liquid output of a low-pressure 180 liter liquid nitrogen dewar. The outflow was dumped into a 25 liter dewar, though very little liquid was collected before the experiment was terminated. The cold shield reached a minimum temperature of -140 C. The center of the chamber, cooled radiatively, reached -20 C before the experiment was stopped. No attempt in this first experiment was made to regulate the shield temperature to near space conditions of -60 C or the pressure to 13 mbar.

Fig. 7 (left) presents chamber temperature data while manually regulating the nitrogen flow with a valve. The PAMSS cage was mounted inside the chamber, with the QCL end well up inside the cold copper shroud. Thermocouples were located on the shroud and at three positions on the PAMSS cage. Nitrogen was turned on at about 60 minutes into the experiment. One sees that the cold shield temperature quickly drops, and then it was possible to manually control the temperature of the shroud fairly well (after a few iterations) to the value expected at the maximum altitude of the balloon flight.

Fig. 7 (right) shows the temperatures from thermistors mounted at three points on the QCL thermal management system. Instead of the QCL, a power resistor was mounted in its place. We see that radiative cooling is so effective, that the radiator side of the TEC is actually colder than the QCL side, whose temperature has fallen well below the 20 C set point. Thus, within about 20 minutes of starting the nitrogen flowing, the pulse-width modulated power to the TEC

cooler drops to zero. When power is applied to the resistor at the QCL position, at the level of our usual QCL average power at ambient conditions, its temperature initially rises, but then falls again. To stabilize the temperature at the desired set-point, which is necessary for spectral stability and the intended function of PAMSS, we will need to run the TEC in reverse or the QCL at higher repetition rate. The data in Fig. 7 (right) simulate the latter, showing that higher average powers at the QCL stabilize QCL temperature at higher values. However, a variable duty cycle on the QCL creates problems by changing its initial temperature before the pulse, which changes its spectrum. Hence it is preferable to control the temperature by heating at altitude. Thus, the lesson learned from this experiment is that the system operating conditions at ambient conditions before the flight and at altitude need to be very different. On the ground, we need to operate the TEC in cooling mode to remove heat from the QCL. At altitude, we need to operate the TEC such that it supplies heat to the QCL.

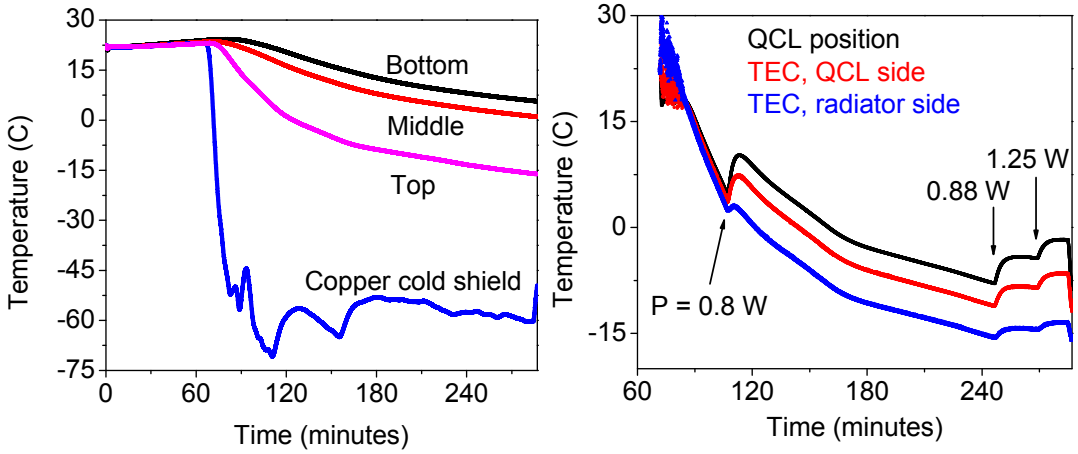

Fig. 7. (left) Temperature data for chamber. (right) Temperature data for QCL thermal management system.

One important result is that our electronics (National Instruments cRIO based) continue to function flawlessly in vacuum and at -15 C ambient temperature with only radiative cooling. We plan to reconfigure the cage system so that heat generated by the electronics can be recycled to help keep the QCL warm.

4. SUMMARY

The test of PAMSS in the NSC environmental chamber had the following successes. By transporting PAMSS across country and operating it in a remote location, completely self-contained with regard to equipment, we have raised the TRL from 4 to 5. Encouraging is that no part of the system failed during vacuum or reduced temperature operation. In particular, the laser alignment was stable. There was no evidence of laser degradation, e.g. of damage to the AR coating by operating in the harsh environment of the chamber. Thermal testing was inconclusive, because the ambient temperature in the chamber never went below 8 C at NSC, and tests in our own chamber have so far included only a dummy load rather than the actual laser. However, the new chamber at UCF has easily reaches near space conditions, and initial experiments using this system have been very informative. We expect to have tested PAMSS at near space conditions and be ready for the scheduled June 2014 balloon flight to 30 km.

ACKNOWLEDGMENTS

This work was supported in part by grants from the Florida Space Institute, Space Florida, a NASA Flight Opportunity Award, and by Higher Committee for Education Development in Iraq (HCED).

REFERENCE

1. "Quantum cascade laser intracavity absorption spectrometer for trace gas sensing," A. V. Muraviev, D. E. Maukonen, C. J. Fredricksen, Gautam Medhi, and R. E. Peale, Appl. Phys. Lett. 103, 091111 (2013).